Angular dependence of resistance and critical current of a Bi-2223 superconducting joint

OPEN ACCESS
IOP Publishing
Superconductor Science and Technology
Supercond. Sci. Technol. **36** (2023) 125010 (9pp)
https://doi.org/10.1088/1361-6668/ad0565

Angular dependence of resistance and critical current of a Bi-2223 superconducting joint

Y Takeda[1,*], G Nishijima[1], U Nakai[2], T Motoki[2], J Shimoyama[2] and H Kitaguchi[1]

[1] National Institute for Materials Science, 3-13 Sakura, Tsukuba, Ibaraki 305-0003, Japan
[2] Department of Physical Sciences, Aoyama Gakuin University, 5-10-1 Fuchinobe, Chuo-ku, Sagamihara, Kanagawa 252-5258, Japan

E-mail: TAKEDA.Yasuaki@nims.go.jp

Received 30 July 2023, revised 3 October 2023
Accepted for publication 20 October 2023
Published 31 October 2023

Abstract

Low resistance and high critical current are prerequisites for superconducting joints used in persistent-mode magnets. Herein, we use a joint resistance evaluation system, previously developed by us, to systematically evaluate the angular dependence of resistance and critical current of a Bi-2223 superconducting joint in a closed-loop sample. The current decay is measured by rotating the sample incrementally. The time dependence of the loop current is evaluated at 4 K, 0.15–0.28 T, and magnetic field angles ranging from 90° to 0, wherein 90° corresponds to the direction parallel to the tape surface. The results suggest that the resistance and critical current of the joint depend on the angle of the magnetic field. The evaluated critical current increases as the angle increases. The angular dependence of resistance can be divided into three regions: low-resistance, transition, and high-resistance regions. The low-resistance region exists at high angles close to 90°. In this region, the decay of the loop current is small, and the persistent current continues to flow. Furthermore, the joint resistance is less than 1.4×10^{-13} Ω. In the transition region, the joint resistance significantly increases by three orders of magnitude with sample rotation. This significant increase is attributed to an increase in the perpendicular component of the magnetic field, which decreases the critical current of the joint. At lower angles, the joint resistance remains high, ranging from 10^{-11} to 10^{-10} Ω. A significant decay in the loop current is observed in the high-resistance region. Based on these findings, we conclude that the design of a persistent-mode magnet must consider not only the magnitude but also the direction of the magnetic field applied to superconducting joints.

Keywords: superconducting joint, HTS, angular dependence, critical current, joint resistance

(Some figures may appear in colour only in the online journal)

* Author to whom any correspondence should be addressed.

1. Introduction

The crystal structure of a cuprate high-temperature superconductor (HTS) is layered with CuO_2 planes sandwiched between charge reservoir layers. Owing to this structure, HTS materials often exhibit anisotropic electromagnetic properties. This anisotropic property is observed in the critical current (I_c) of an HTS tape when a magnetic field is applied in various directions, that is, the angular dependence of I_c. Commercially available $REBa_2Cu_3O_y$ (REBCO, RE = rare earth) and $(Bi,Pb)_2Sr_2Ca_2Cu_3O_y$ (Bi-2223) HTS tapes exhibit a strong angular dependence of I_c [1–5]. In a superconducting magnet, the magnetic field is applied in various directions to superconducting wires/tapes. Superconducting magnets using HTS tapes have been designed to account for the angular dependence [6–9].

Superconducting joints are used in persistent-mode magnets [10, 11]. Both high joint I_c (I_{cj}) and low joint resistance (R_j) are required for a superconducting joint. Over the past decade, significant progress has been made in superconducting joint technology for HTS tapes/wires [11–21].

The value of I_{cj} is typically evaluated using a transport measurement, similar to the I_c measurement of a superconducting tape/wire. In-field I_{cj} values of REBCO and Bi-2223 samples have been reported with the magnetic field perpendicular or parallel to the surface of the joined tape [18, 20, 22–24]. However, in practice, the direction of the magnetic field applied to the superconducting joints in a persistent-mode magnet is not necessarily perpendicular or parallel. Therefore, the angular dependence of I_{cj} for REBCO and Bi-2223 superconducting joints must be investigated in detail not only for the precise design of a persistent-mode magnet but also for a deeper understanding of materials science involved in HTS joints.

Low R_j is another important property of a superconducting joint. R_j of 10^{-13}–10^{-14} Ω is achieved in a routinely manufactured Nb-Ti superconducting joint for commercial magnetic resonance imaging persistent-mode magnets [10]. For a persistent-mode 30.5 T (1.3 GHz) nuclear magnetic resonance (NMR) magnet that we are developing, R_j of less than 10^{-12} Ω at the operating current of 231 A is required for a superconducting joint between HTS tapes [11, 25, 26]. Several studies have evaluated the R_j of HTS joints [12, 14–16, 18, 20, 21, 24–30]. However, to the best of our knowledge, no studies on the angular dependence of R_j have been reported so far.

Transport measurements, which are used to evaluate in-field I_{cj}, are usually used to evaluate resistance. However, the lower limit of R_j that can be evaluated by the transport measurement is approximately 10^{-11} Ω [31, 32]. Therefore, these measurements cannot be used to evaluate the low resistance of a superconducting joint. Generally, the current decay method is typically used to evaluate R_j of less than 10^{-11} Ω [10, 33–41]. This method requires a closed loop comprising a superconducting tape/wire with a superconducting joint connecting both ends of the tape/wire. The decay of the current introduced in the superconducting loop (I_{loop}) is measured. An initial fast decay of I_{loop} is typically observed owing to the current-sharing effect [33, 35, 36, 40, 41]. After the fast decay is settled, a subsequent slow decay of I_{loop} is observed. Assuming that R_j is constant and corresponds to the circuit resistance, the time (t) dependence of I_{loop} in the slow decay can be described as follows:

$$I_{loop}(t) = I_{loop}(0) \exp\left(-\frac{R_j}{L}t\right), \quad (1)$$

where L is the self-inductance of the loop [10, 33].

The magnetic field is typically measured to evaluate I_{loop}. Mostly, the center field trapped in the loop is measured using a Hall sensor. A superconducting quantum interference device voltmeter or magnetometer is occasionally used to improve the measurement sensitivity [35, 40].

We have previously developed a joint resistance evaluation system that enables efficient current decay measurements [42]. In that system, a closed-loop sample is cooled using a pulse-tube cryocooler. The loop diameter in each sample is 100 mm. The number of turns in the loop is typically one, but more than one turn is acceptable. The value of L of the one-turn loop is 0.47 μH. The I_{loop} is introduced via magnetic induction using a copper coil located at the center of the loop.

In our measurements, the magnetic field near the superconducting tape/wire, the so-called 'self-field,' was measured using the Hall sensor to evaluate I_{loop}. This is because the self-field is larger than the center field of the loop. The measurement sensitivity of this method is sufficient to evaluate the decay of I_{loop}. However, uncertainty exists in the absolute value of I_{loop} obtained from the measured magnetic field, particularly when the loop consists of a tape. To reduce uncertainty and improve precision, we have previously developed a current sensor consisting of a split core made of laminated electromagnetic steel and a Hall sensor [30].

Using this system, if the introduced I_{loop} is sufficiently lower than I_{cj}, R_j value less than 10^{-13} Ω can be evaluated by measuring the current decay for several tens of minutes. If the introduced I_{loop} is close to or exceeds I_{cj}, I_{cj} value can be evaluated using the time dependence of the I_{loop} or residual I_{loop} observed after stabilizing the current decay. We have evaluated not only R_j but also I_{cj} for various superconducting loops using this system [20, 30, 42–45].

Previously, we combined this system with a superconducting solenoid magnet to evaluate R_j in a vertical magnetic field [30]. Recently, we introduced a split-pair superconducting magnet instead of the solenoid. This split-pair magnet applies a horizontal magnetic field (B) to the joint, as shown in figure 1(a). A system consisting of a motor and gears was implemented to rotate the closed-loop sample around the vertical axis. These enable us to evaluate the angular dependence of R_j and I_{cj}.

To ensure the design of a Bi-2223 persistent-mode magnet, it is crucial to evaluate the angular dependence of R_j and I_{cj}, because I_{cj} may lack sufficient margin. In this study, we evaluated the angular dependence of R_j and I_{cj} in a Bi-2223 closed-loop sample with a superconducting joint. We

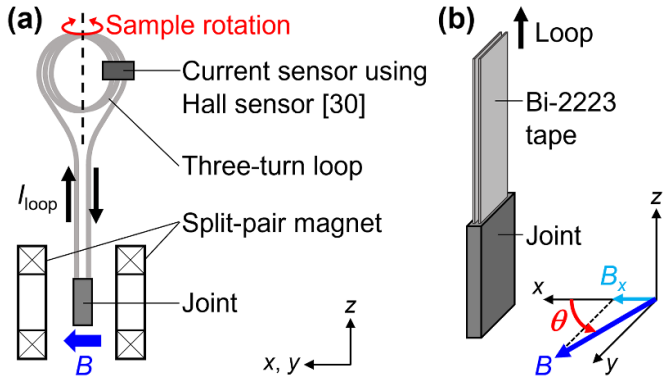

Figure 1. (a) Schematic of experimental setup. Horizontal magnetic field (B) is applied to the joint using a split-pair superconducting magnet. The direction of magnetic field is controlled by rotating the sample. (b) Schematic showing the angle of magnetic field (θ). The perpendicular component of the magnetic field applied to the tape surface is B_x ($=B\cos\theta$).

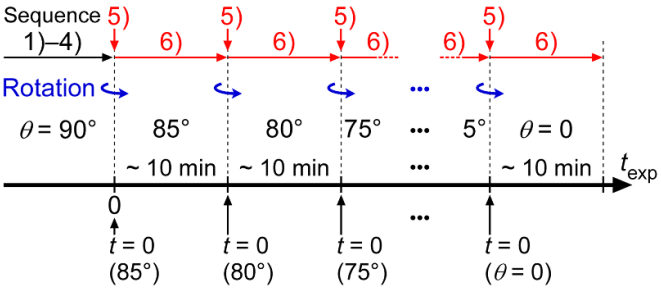

Figure 2. Schematic of the sequence for measuring the current decay by incrementally rotating the sample. In sequence (5), the sample is rotated by 5° within 1 s. At each angle, t is the elapsed time from when we started sample rotation. In sequences (6) and (7), we measured the current decay for approximately 10 min at each angle from 0 to 85°.

combined current decay measurements and sample rotation. To the best of our knowledge, this is the first systematic evaluation of the angular dependence of R_j and I_{cj} of an HTS joint.

2. Method

2.1. Sample fabrication

We fabricated a Bi-2223 closed-loop sample with a superconducting joint shown in figure 1(a). A 1.6 m long Ni-alloy-reinforced Bi-2223/Ag tape (DI-BSCCO® Type HT-NX [2, 4, 46, 47]) was used. The width and thickness of the tape were 4.5 and 0.25 mm, respectively. The reinforcement at both ends, approximately 0.2 m long, was removed [26]. A praying-hands-type superconducting joint was formed to connect both ends using a previously reported process [17, 20, 45].

To form the superconducting joint, a polycrystalline Bi-2223 intermediate layer was synthesized via heat treatment. As described in our previous study [45], during heat treatment, the sample was a one-turn loop with an approximately 0.6 m long temperature transition zone. The joint was inserted into a tube furnace and heat-treated, whereas the loop part with the reinforcement was placed outside the furnace and held at room temperature. After the heat treatment, the one-turn loop was wound into a three-turn loop with a diameter of 100 mm. The L of the sample was 1.4 μH, which was measured at room temperature before the ends were connected [42].

2.2. Current decay measurements with sample rotation

Current decay was measured by rotating the sample incrementally. The angle of the magnetic field (θ) was determined as shown in figure 1(b). The direction of the magnetic field at $\theta = 90°$ was parallel to the tape surface. The time dependence of the voltage of the Hall sensor (V_{Hall}) in the current sensor was measured at each angle. I_{loop} was calculated from V_{Hall} using a linear relationship between a current and V_{Hall} obtained experimentally beforehand [20, 30].

In a preliminary experiment, I_{cj} reached the maximum at 90°. We started to rotate the sample (decrease θ) from 90° at the experimental time (t_{exp}) of 0. At each angle, t was the elapsed time from when we started sample rotation. The measurement sequence, schematically shown in figure 2, is described as follows:

(1) The temperature of the sample was controlled to be 4 K.
(2) A magnetic field (B) of 0.15–0.28 T was applied to the joint at 90°.
(3) An I_{loop} of 220–221 A was introduced to the sample.
(4) We waited until the initial current-sharing effect in the sample became negligible and the time variation V_{Hall} became flat, which required several tens of minutes.
(5) The sample was rotated (θ was decreased) by 5° within 1 s while the I_{loop} flowed. At $t_{exp} = 0$, the sample was rotated from 90° to 85°. This point corresponded to $t = 0$ at 85°.
(6) The time dependence of V_{Hall} was measured for approximately 10 min.
(7) The 5° rotation and the 10 min measurement were repeated until $\theta = 0$.

Using the measured V_{Hall}, we obtained the time dependence of I_{loop} (I_{loop}–t) for approximately 10 min at each angle. Because we measured V_{Hall} at a sampling rate of 1 Hz, there were typically more than 600 data points in each I_{loop}–t curve.

2.3. Evaluation of R_j and I_{cj}

To evaluate R_j and I_{cj} at each 5°-incremental angle between 0 and 85°, we used 300 data points of the I_{loop}–t curve at 300 s $\leqslant t \leqslant$ 600 s. At 90°, R_j was evaluated using 300 data points at -300 s $\leqslant t_{exp} \leqslant 0$.

The value of R_j was obtained by fitting the data points of the I_{loop}–t curve to equation (1) using the least squares method. The value of I_{cj} was estimated using the I_{loop} dependence of the voltage (V) obtained from the I_{loop}–t curve. When current

decay was observed, we could calculate V using equation (2) as follows:

$$V = -L\frac{\Delta I_{\mathrm{loop}}}{\Delta t}. \quad (2)$$

The I_{loop} dependence of the calculated voltage (V–I_{loop}) was smoothed using a 15-point moving average. The smoothed V–I_{loop} curve at a voltage ranging from 10^{-7} to 10^{-9} V was fitted to an empirical power law model ($V = \alpha\, {I_{\mathrm{loop}}}^{n}$, where α and n are constants) using the least squares method. We estimated I_{cj} at a voltage criterion (V_{c}) of 10^{-8} V, which corresponded to the I_{loop} value at $V = 10^{-8}$ V. Some of the I_{loop} values at 10^{-8} V were estimated by the extrapolation from the fitting.

3. Results and discussion

3.1. Time dependence of I_{loop} obtained from V_{Hall}

Figure 3 shows V_{Hall} as a function of t_{exp} at 4 K and 0.25 T. The inset shows the magnified view at approximately 70°. From 90° to 75°, a decrease in V_{Hall} with time was not clearly observed; that is, V_{Hall}–t_{exp} at each angle was almost flat. This implies that the decay of I_{loop} was negligible at 75–90°, and the I_{loop} was considerably lower than I_{cj}. By contrast, at angles less than 75°, a decrease in V_{Hall} over time was evident.

The value of V_{Hall} increased by less than 1 mV for each 5° rotation, as shown in the inset of figure 3. There are two possible reasons for this increase in V_{Hall}: the first is the static component of the change in the offset of V_{Hall}. The offset is primarily attributed to the leakage field of the split-pair magnet, calculated to be approximately 1 mT in the direction opposite to the magnetic field applied to the joint. The thin-film Hall sensor used in the current sensor was parallel to the plane of the Bi-2223 tape in the loop. The offset was approximately 0.6 mV at 90° and increased with sample rotation. At $\theta = 0$, this static component showed the largest value of 3.7 mV. The second reason is the dynamic component showing an increase in I_{loop} owing to magnetic induction. The magnetic flux across the loop of the sample owing to the leakage field is reduced by sample rotation. This reduction in magnetic flux induces a current in the loop. This induced current increases I_{loop}, resulting in an increase in V_{Hall}.

The time variation of I_{loop}, I_{loop}–t, at 4 K, 0.25 T, and each angle of 0–85° is shown in figure 4(a). The I_{loop} values were obtained from the V_{Hall} values shown in figure 3. The offset was subtracted from V_{Hall} at each angle.

Figure 4(a) shows that, at angles less than 70°, the residual I_{loop}, that is, the I_{loop} at 600 s decreased as the angle decreased. This corresponds to a decrease in I_{cj}. Sample rotation from high to low angle between 90° and 0 increased the perpendicular component of the magnetic field applied to the tape surface, that is, B_x ($=B\cos\theta$) shown in figure 1(b). Because the intermediate layer was formed almost parallel to the tape surface [20], B_x was almost perpendicular to the intermediate layer of the superconducting joint. Furthermore, because Bi-2223

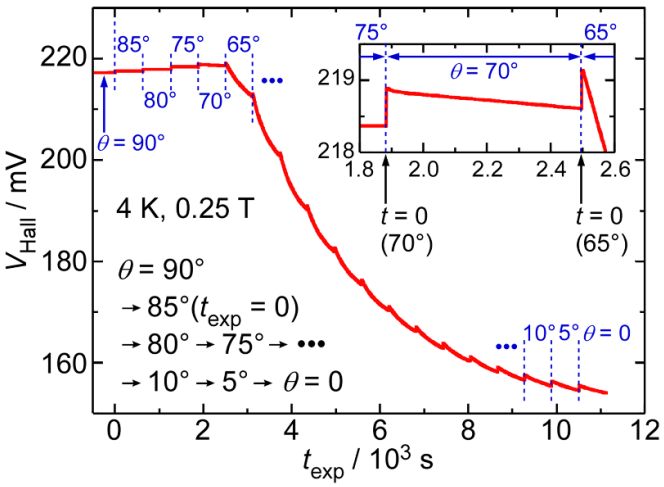

Figure 3. Voltage of Hall sensor (V_{Hall}) in the current sensor as a function of experimental time (t_{exp}) at 4 K and 0.25 T. We started to rotate the sample from 90° at $t_{\mathrm{exp}} = 0$ by 5° within 1 s. Inset shows a magnified view at approximately 70°.

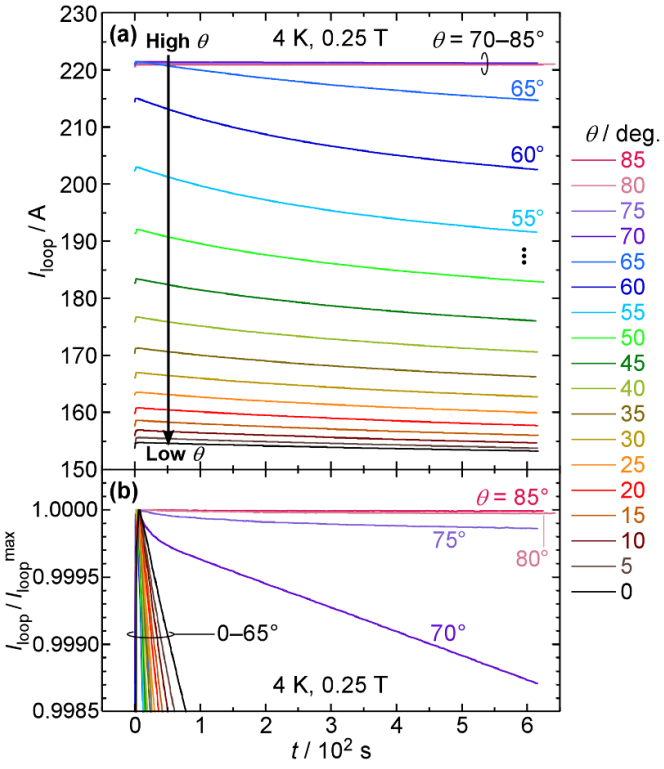

Figure 4. Time dependence of (a) I_{loop} and (b) normalized I_{loop} at 4 K, 0.25 T, and 0–85°. I_{loop} values are calculated using V_{Hall} values shown in figure 3. At angles less than 70°, I_{loop} at 600 s decreases as the angle decreases owing to a decrease in I_{cj}. A persistent current continues to flow in the sample at high angles of 75–90°.

grains in the intermediate layer were weakly c-axis-aligned [45, 48], B_x was almost parallel to the c-axis of these grains. As B_x increased, I_{c} of the intermediate layer decreased significantly. Because I_{cj} was primarily dominated by the I_{c} of the intermediate layer [48], I_{cj} decreased as the angle decreased and B_x ($=B\cos\theta$) increased.

Figure 4(b) shows the normalized I_{loop} using the maximum value ($I_{loop}{}^{max}$) at each angle. The decay ratio ($1 - I_{loop}/I_{loop}{}^{max}$) at 75° for 600 s was 1.4×10^{-4}. The field drift rate is less than 10^{-2} ppm h^{-1} in a typical 400 MHz (9.4 T) Nb-Ti NMR magnet with 10 joints and L of 40 H at an operating current of approximately 100 A [10]. If the performance of the 10 joints is equivalent to that of the Bi-2223 superconducting joint sample at 75°, a field drift rate of 2.9×10^{-4} ppm h^{-1} can be extrapolated. This rate is considerably lower than that of the typical NMR magnet. Consequently, a persistent current continued to flow in the sample at 4 K, 0.25 T, and high angles of 75–90°.

The decay ratio at 70° for 600 s was 1.3×10^{-3}. This corresponds to a field drift rate of 2.7×10^{-3} ppm h^{-1} using the same extrapolation. Although this value is close to that of the typical NMR magnet, the decay of I_{loop} at 70° is clearer than at 75°, as shown in figure 4(b). Therefore, we conclude that a persistent current did not flow at 0–70°.

3.2. Angular dependence of I_{cj} and R_j

Figures 5(a)–(d) shows the angular dependence of I_{cj} and R_j at 4 K for 0.15, 0.20, 0.25, and 0.28 T, respectively. The vertical error bars for R_j, which are visible at 85° and 90° in figure 5(c), correspond to the standard uncertainty obtained from fitting. At 0.15 and 0.20 T, the measurements at high angles close to 90° were performed at intervals of 15° and 10°, respectively. This is because I_{loop} was expected to be considerably lower than I_{cj}, which caused negligible current decay.

At a certain angle, I_{cj} decreased as the magnetic field increased. This was consistent with the field dependence of I_{cj} evaluated by transport measurements using a Bi-2223 superconducting joint sample [20]. The evaluated I_{cj} increased as the angle increased. The I_{cj} probably showed a broad peak at 90°, similar to the angular dependence of I_c for Bi-2223 tapes [1, 5].

Figure 6 shows the smoothed V–I_{loop} curve at 0.15 T and 0–50°. We calculated the voltage from the I_{loop}–t curve at 300 s $\leqslant t \leqslant$ 600 s using equation (2). When the decay of I_{loop} is significant, ΔI_{loop} becomes large and the calculated voltage is also large. The range of the calculated voltage varies with the angle. From the obtained V–I_{loop} curve, I_{cj} was evaluated at V_c of 10^{-8} V for each angle. At 25–40°, I_{cj} was obtained from the intersection of V–I_{loop} and V_c, because V_c was within the voltage range of V–I_{loop}. At 0–20°, the V–I_{loop} curves were extrapolated using the power law ($V = \alpha\, I_{loop}{}^{n}$) as shown by dashed lines in figure 6 because the voltage range was lower than V_c. I_{cj} was estimated from the intersection of the extrapolated V–I_{loop} and V_c.

At 45° and 50°, the I_{cj} values estimated from the intersections were higher than the initially introduced I_{loop} of 220 A. Given that I_{cj} was estimated from the current decay, I_{cj} values higher than the initial I_{loop} value were not realistic. Thus, for 0.15 T, we employed I_{cj} only at 0–40°.

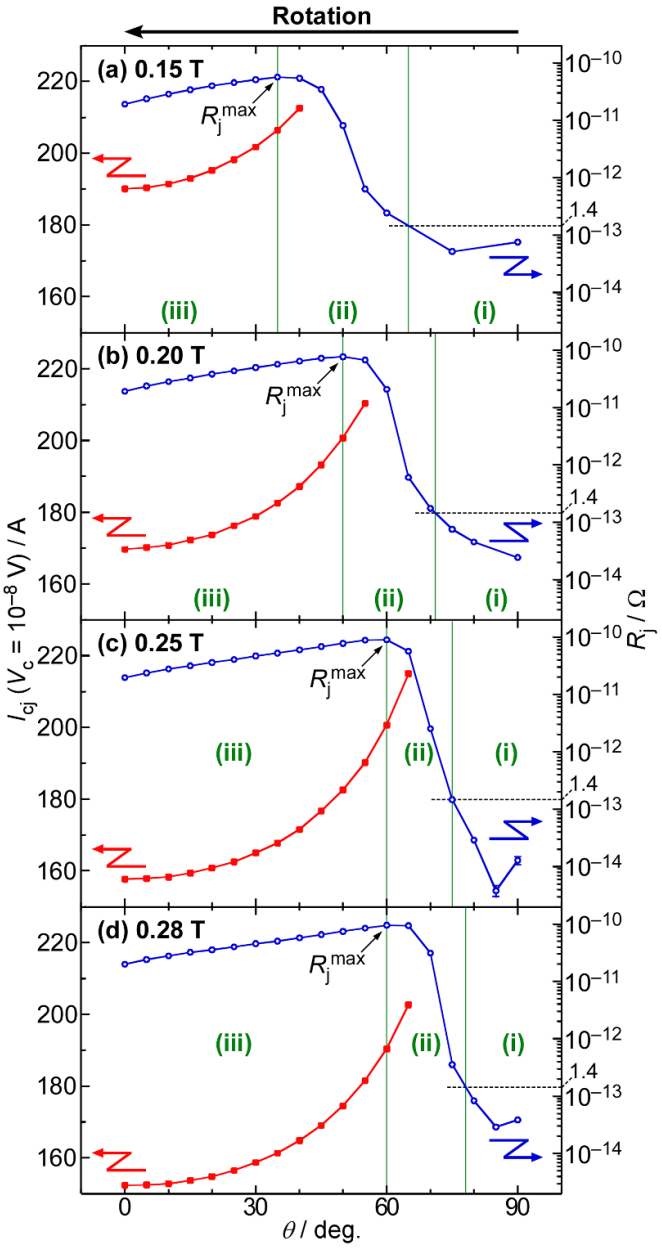

Figure 5. Angular dependence of R_j and I_{cj} at 4 K for (a) 0.15 T, (b) 0.20 T, (c) 0.25 T, and (d) 0.28 T. Vertical error bars for R_j correspond to the standard uncertainty obtained from fitting. I_{cj} increases as the angle increases. The angular dependence of R_j with sample rotation can be divided into three regions: (i) low-resistance region (R_j of less than 1.4×10^{-13} Ω), (ii) transition region (three orders of magnitude change in R_j to its maximum, $R_j{}^{max}$), and (iii) high-resistance region (R_j of 10^{-11}–10^{-10} Ω).

The I_{cj} values were evaluated in a similar way for 0.20, 0.25, and 0.28 T. I_{cj} values lower than the initial I_{loop} value (220 A) are shown in figure 5. This is the reason why I_{cj} at higher angles are not plotted.

The angular dependence of R_j with sample rotation can be divided into three regions: (i) low-resistance region (R_j of less than 1.4×10^{-13} Ω), (ii) transition region (three orders of magnitude changes in R_j to its maximum, $R_j{}^{max}$), and

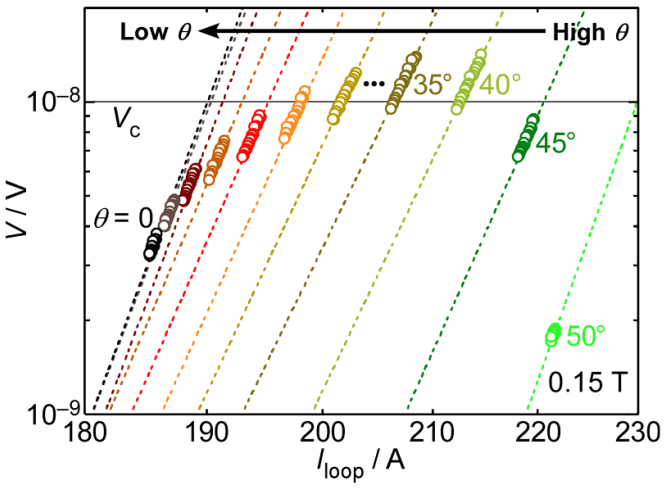

Figure 6. Smoothed V–I_{loop} curve at 0.15 T and 0–50°. V–I_{loop} at 0–50° is fitted to the power law model, as shown by dashed lines.

(iii) high-resistance region (R_j of 10^{-11}–10^{-10} Ω). The angular dependence of R_j in each region is discussed below.

(i) Low-resistance region

This region is observed at high angles for each magnetic field. Figure 4(b) shows that the decay of I_{loop} at 75–90° and 0.25 T, corresponding to this region, was small. Because I_{loop} is considerably lower than I_{cj}, low R_j is realized and the persistent current continues to flow, as described in the previous section.

At 0.25 T and 75°, R_j was evaluated to be 1.4×10^{-13} Ω. The coefficient of determination (r^2) in the fitting using the least squares method was 0.99. This implies that R_j can be obtained quantitatively. However, r^2 decreased at higher angles of 80–90° for 0.25 T, at which the lower R_j values were observed. As shown in figure 4(b), the I_{loop}–t curves were nearly flat at these angles. Although not visible in figure 3, the noise of V_{Hall} of $\pm 5 \times 10^{-7}$ V influenced the I_{loop}–t curves, corresponding to ±2 ppm deviation in I_{loop}. Consequently, the uncertainty in the fitting for R_j derivation was large.

In region (i), for R_j of less than 4×10^{-14} Ω, r^2 was less than 0.8. This indicates that such low R_j values could not be quantitatively evaluated. Nevertheless, it is certain that the R_j values were less than the quantitative value of 1.4×10^{-13} Ω at 0.25 T and 75°. This indicates that the persistent current continued to flow in the sample owing to sufficiently low R_j.

(ii) Transition region

The value of R_j changed by approximately three orders of magnitude to its maximum (R_j^{max}) in region (ii). Its values were evaluated quantitatively because r^2 was larger than 0.98 for each fitting.

As shown in figure 5, region (ii) shifted toward higher angles as the magnetic field increased. To clarify this shift, sections of R_j in region (ii) of figures 5(a)–(d) are shown in figure 7(a). Figure 7(b) shows this plot with the horizontal axis changed to $B\cos\theta$. The significant change in R_j at each magnetic field was nearly identical at $B\cos\theta$ of 6–11 $\times 10^{-2}$ T. The changes in R_j were independent of the magnitude of magnetic field.

As described in the previous section, I_{cj} decreased owing to sample rotation with an increase in $B_x = B\cos\theta$. R_j is known to increase as the ratio of I_{loop} to I_{cj} increases, that is, as the load factor increases [30, 36, 38, 42]. In region (ii), the changes in R_j were due to the following reason. I_{cj} decreased as $B_x = B\cos\theta$ increased owing to sample rotation. Because the change in I_{loop} by sample rotation is small, this decrease in I_{cj} caused an increase in the load factor. This resulted in a significant increase in R_j. The load factor values were not calculated, because I_{cj} could not be evaluated at most angles for each magnetic field in region (ii).

(iii) High-resistance region

This region eventually appeared when θ approached zero with sample rotation. High R_j values of 10^{-11}–10^{-10} Ω corresponded to the decay of I_{loop} by several amperes, as shown in figure 4(a).

In region (iii), r^2 in the fitting ranged from 0.99 to 1.00, indicating that the R_j values were valid with sufficient precision. As shown in figure 5, R_j was higher at higher angles in each magnetic field. Using the evaluated I_{cj} values in region (iii), we quantitatively discussed the relationship between the load factor (F) and R_j. The value of F was calculated using equation (3) as follows:

$$F = \frac{I_{loop}\,(t = 450\,\mathrm{s})}{I_{cj}\left(V_c = 10^{-8}\,\mathrm{V}\right)}, \tag{3}$$

where $t = 450$ s corresponds to the median of the range of t used to obtain R_j (300 s $\leqslant t \leqslant$ 600 s). The value of F can be larger than 1.00 when I_{loop} ($t = 450$ s) exceeds I_{cj}, because I_{cj} is determined by a considerably low voltage criterion, $V_c = 10^{-8}$ V.

Figure 8 shows the relationship between F and R_j in region (iii), where the gray dashed line is derived using the least squares method. The value of F increased as the angle increased. The F values of 0.974–1.02 suggest that I_{loop} was comparable to I_{cj}. For F values of 0.974–1.02, R_j appeared to increase linearly. This suggests that, in region (iii), the change in R_j owing to sample rotation is primarily attributed to the change in F.

3.3. Discussion

When the sample is rotated, I_{loop} is probably influenced by the screening current and current sharing in the sample. The screening current is induced by sample rotation owing to an increase in B_x. Current sharing occurs when I_{loop} is close to or exceeds I_{cj}, typically in regions (ii) and (iii). However, as described in the previous section, the behavior of R_j could be explained using $B\cos\theta$ and F in regions (ii) and (iii),

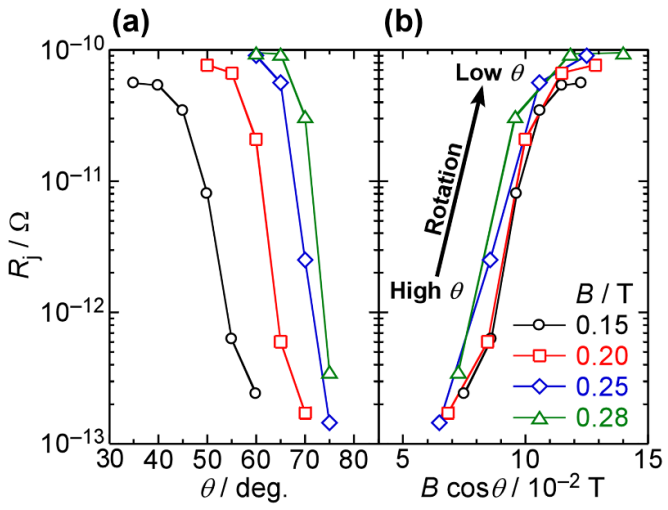

Figure 7. (a) Sections of R_j in region (ii) of figures 5(a)–(d). Region (ii) shifts toward higher angles as the magnetic field increases. (b) Relationship between $B\cos\theta$ and R_j in region (ii). The significant changes in R_j at each magnetic field are nearly identical at $B\cos\theta$ of 6–11 × 10^{-2} T, which are independent of the magnitude of the magnetic field.

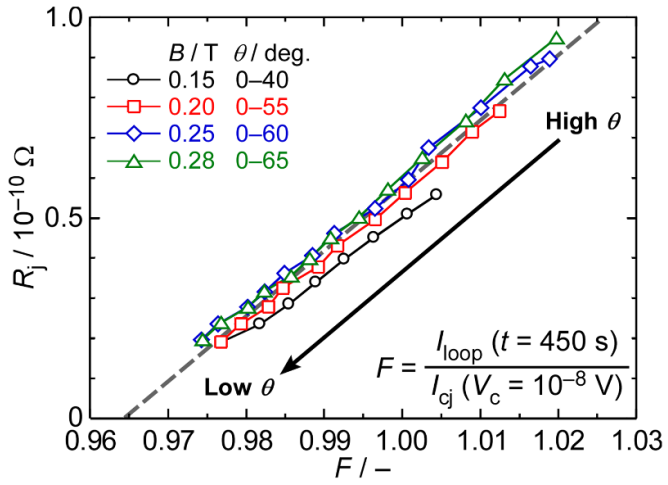

Figure 8. Relationship between load factor (F) and R_j in region (iii). Change in R_j owing to sample rotation is primarily attributed to change in F.

respectively. This implies that the influences of the screening current and current sharing were sufficiently small in our measurements.

As explained in 3.2, we employed the I_{cj} values lower than the initially introduced I_{loop} of 220 A. Therefore, the highest angle at which I_{cj} was obtained was 65° at 0.25 and 0.28 T. If a larger I_{loop} is introduced, larger I_{cj} values can be evaluated at high angles near 90°.

In a preliminary measurement at 0.3 T, an introduced I_{loop} of 220 A decayed even at 90°. A persistent current of 220 A did not flow at 0.3 T. This means that region (i) was not observed at 0.3 T. To investigate the resistance transition from regions (i)–(iii) in this study, we chose 0.28 T as the maximum magnetic field.

At present, I_{cj} (I_c of the Bi-2223 superconducting joint) is lower than I_c of a tape [2, 4]. To ensure sufficient current margin, superconducting joints must be placed in a space at a low magnetic field in a magnet. In the 1.3 GHz (30.5 T) NMR magnet being developed, the magnetic field applied to the Bi-2223 superconducting joints is designed to be lower than 1 T [11, 25]. We believe that the magnetic fields of 0.15–0.28 T used in this study are in a realistic range for practical applications.

The angular dependence of R_j suggests that, in the design of a persistent-mode magnet, we must consider not only the magnitude but also the direction of a magnetic field applied to superconducting joints. The magnet must be designed such that superconducting joints are used in region (i). This allows for persistent-mode operation with a low R_j. If superconducting joints must be used in regions (ii) or (iii), additional efforts must be made to achieve a lower R_j. A recent study has shown that when I_{loop} is close to I_{cj}, R_j is almost inversely proportional to the elapsed time and decreases with an increase in the pinning potential of a superconducting joint [49]. This may be effective for achieving a lower R_j.

In region (iii), R_j decreased as F decreased. The relationship between F and R_j shown in figure 8 implies that a low R_j, as observed in region (i), may be achieved at F of less than 0.964. Evaluating the trend of R_j in detail at F equal to approximately 0.964 will help clarify the conditions under which a sufficiently low R_j for a persistent-mode operation can be achieved.

4. Conclusion

In this study, the angular dependence of R_j and I_{cj} of a Bi-2223 closed-loop sample with a superconducting joint was systematically evaluated at 4 K and 0.15–0.28 T. An evaluation method combining current decay measurements and sample rotation was used. The sample was rotated from 90° to 0, wherein the angle of 90° corresponded to the direction of the magnetic field parallel to the tape surface. The following conclusions were drawn:

(1) R_j and I_{cj} are dependent on the angle of the magnetic field. The evaluated I_{cj} increased as the angle increased. The angular dependence of R_j with sample rotation can be divided into three regions:
   (i) In the low-resistance region, corresponding to high angles close to 90°, the loop current was considerably lower than I_{cj}. R_j of less than 1.4 × 10^{-13} Ω was observed and a persistent current continued to flow in the sample.
   (ii) In the transition region, R_j significantly increased by three orders of magnitude owing to an increase in the perpendicular component of the magnetic field, which decreased I_{cj}. This caused an increase in the ratio of the loop current to I_{cj}, that is, the load factor, resulting in an increase in R_j.

(iii) In the high-resistance region, corresponding to low angles, R_j remained high, ranging from 10^{-11} to 10^{-10} Ω. When the load factor was 0.974–1.02, R_j appeared to increase linearly.

(2) In the design of a persistent-mode magnet, we must consider not only the magnitude but also the direction of a magnetic field applied to superconducting joints. Evaluating the trend of R_j in detail at the load factor of approximately 0.964 will help clarify the conditions under which a sufficiently low R_j for a persistent-mode operation can be achieved.

Data availability statement

All data that support the findings of this study are included within the article (and any supplementary files).

Acknowledgments

This work was supported by JST Mirai-Program Grant No. JPMJMI17A2 and JSPS KAKENHI Grant No. JP22K14482, Japan.

ORCID iDs

Y Takeda https://orcid.org/0000-0001-7217-9853
G Nishijima https://orcid.org/0000-0001-7493-0559
T Motoki https://orcid.org/0000-0003-3218-0977
J Shimoyama https://orcid.org/0009-0007-1783-676X

References

[1] Sunwong P, Higgins J S and Hampshire D P 2011 Angular, temperature, and strain dependence of the critical current of DI-BSCCO tapes in high magnetic fields *IEEE Trans. Appl. Supercond.* **21** 2840–4

[2] Miyoshi Y, Nishijima G, Kitaguchi H and Chaud X 2015 High field Ic characterizations of commercial HTS conductors *Physica* C **516** 31–35

[3] Tsuchiya K *et al* 2016 Critical current characterization of commercial REBCO coated conductors at 4.2 and 77 K *IEEE Trans. Appl. Supercond.* **27** 6600205

[4] Bonura M, Barth C and Senatore C 2019 Electrical and thermo-physical properties of Ni-alloy reinforced Bi-2223 conductors *IEEE Trans. Appl. Supercond.* **29** 6400205

[5] Kobayashi D, Okada T and Awaji S 2022 High-field critical current properties of $(Bi,Pb)_2Sr_2Ca_2Cu_3Oy$ filaments *IEEE Trans. Appl. Supercond.* **32** 6400105

[6] Uglietti D, Kitaguchi H, Choi S and Kiyoshi T 2009 Angular dependence of critical current in coated conductors at 4.2 K and magnet design *IEEE Trans. Appl. Supercond.* **19** 2909–12

[7] Kiyoshi T, Choi S, Matsumoto S, Zaitsu K, Hase T, Miyazaki T, Hamada M, Hosono M and Maeda H 2011 Bi-2223 Innermost coil for 1.03 GHz NMR magnet *IEEE Trans. Appl. Supercond.* **21** 2110–3

[8] Matsumoto S, Kiyoshi T, Otsuka A, Hamada M, Maeda H, Yanagisawa Y, Nakagome H and Suematsu H 2012 Generation of 24 T at 4.2 K using a layer-wound GdBCO insert coil with Nb_3Sn and Nb–Ti external magnetic field coils *Supercond. Sci. Technol.* **25** 025017

[9] Nishijima G, Kitaguchi H, Tsuchiya Y, Nishimura T and Kato T 2013 Transport critical current measurement apparatus using liquid nitrogen cooled high-Tc superconducting magnet with variable temperature insert *Rev. Sci. Instrum.* **84** 015113

[10] Brittles G D, Mousavi T, Grovenor C R M, Aksoy C and Speller S C 2015 Persistent current joints between technological superconductors *Supercond. Sci. Technol.* **28** 093001

[11] Takeda Y, Maeda H, Ohki K and Yanagisawa Y 2022 Review of the temporal stability of the magnetic field for ultra-high field superconducting magnets with a particular focus on superconducting joints between HTS conductors *Supercond. Sci. Technol.* **35** 043002

[12] Park Y, Lee M, Ann H, Choi Y H and Lee H 2014 A superconducting joint for $GdBa_2Cu_3O_{7-\delta}$-coated conductors *NPG Asia Mater.* **6** e98

[13] Jin X, Yanagisawa Y, Maeda H and Takano Y 2015 Development of a superconducting joint between a $GdBa_2Cu_3O_{7-\delta}$-coated conductor and $YBa_2Cu_3O_{7-\delta}$ bulk: towards a superconducting joint between RE (Rare Earth) $Ba_2Cu_3O_{7-\delta}$-coated conductors *Supercond. Sci. Technol.* **28** 075010

[14] Ohki K *et al* 2017 Fabrication, microstructure and persistent current measurement of an intermediate grown superconducting (iGS) joint between REBCO-coated conductors *Supercond. Sci. Technol.* **30** 115017

[15] Chen P *et al* 2017 Development of a persistent superconducting joint between Bi-2212/Ag-alloy multifilamentary round wires *Supercond. Sci. Technol.* **30** 025020

[16] Mukoyama S, Nakai A, Sakamoto H, Matsumoto S, Nishijima G, Hamada M, Saito K and Miyoshi Y 2018 Superconducting joint of REBCO wires for MRI magnet *J. Phys.: Conf. Ser.* **1054** 012038

[17] Takeda Y, Motoki T, Kitaguchi H, Nakashima T, Kobayashi S, Kato T and Shimoyama J 2019 High Ic superconducting joint between Bi2223 tapes *Appl. Phys. Express* **12** 023003

[18] Jin X, Suetomi Y, Piao R, Matsutake Y, Yagai T, Mochida H, Yanagisawa Y and Maeda H 2019 Superconducting joint between multi-filamentary $Bi_2Sr_2Ca_2Cu_3O_{10+\delta}$ tapes based on incongruent melting for NMR and MRI applications *Supercond. Sci. Technol.* **32** 035011

[19] Mousavi T, Santra S, Melhem Z, Speller S and Grovenor C 2021 Superconducting joint structures for Bi-2212 wires using a powder-in-tube technique *IEEE Trans. Appl. Supercond.* **31** 6400504

[20] Takeda Y *et al* 2022 Critical current improvement and resistance evaluation of superconducting joint between Bi2223 tapes *Supercond. Sci. Technol.* **35** 02LT02

[21] Huang D, Shang H, Xie B, Zou Q, Dong H, Wang K, Zhang L, Gu H and Ding F 2022 An efficient approach for superconducting joint of YBCO coated conductors *Supercond. Sci. Technol.* **35** 075004

[22] Kim S B, Saito R, Takahashi M, Park Y J, Lee M H, Oh Y K and Noguchi S 2016 Shape optimization of the stacked HTS double pancake coils for compact NMR relaxometry operated in persistent current mode *IEEE Trans. Appl. Supercond.* **26** 43017004

[23] Nishijima G, Matsumoto S, Nakai A, Sakamoto H, Mukoyama S, Miyoshi Y, Saito K and Hamada M 2019 Transport property of REBCO superconducting joints in magnetic fields at various temperatures *IEEE Trans. Appl. Supercond.* **29** 6602105

[24] Yanagisawa Y *et al* 2021 Development of a persistent-mode NMR magnet with superconducting joints between

high-temperature superconductors *Supercond. Sci. Technol.* **34** 115006
[25] Maeda H, Shimoyama J, Yanagisawa Y, Ishii Y and Tomita M 2019 The MIRAI program and the new super-high field NMR initiative and its relevance to the development of superconducting joints in Japan *IEEE Trans. Appl. Supercond.* **29** 4602409
[26] Takeda Y *et al* 2022 Development of a persistent current mode 9.39 T (400 MHz) LTS/Bi-2223 NMR magnet with a Bi-2223 superconducting joint *IEEE Trans. Appl. Supercond.* **32** 4301005
[27] Jin X, Yanagisawa Y and Maeda H 2018 Measurement of persistent current in a Gd123 coil with a superconducting joint fabricated by the CJMB method *IEEE Trans. Appl. Supercond.* **28** 4602604
[28] Takahashi K, Hase T, Awaji S, Nakai A, Yamano S, Mukoyama S and Sakamoto H 2018 Performance of an HTS persistent current system for REBCO pancake coil *IEEE Trans. Appl. Supercond.* **28** 4600104
[29] Matsumoto S, Nishijima G, Nakai A, Sakamoto H, Mukoyama S, Miyoshi Y, Saito K and Hamada M 2019 Estimation of joint resistance in REBCO single-turn loop under magnetic fields *IEEE Trans. Appl. Supercond.* **29** 4602005
[30] Kobayashi K, Nishijima G, Ohki K, Nagaishi T, Uchida A and Kitaguchi H 2022 In-field evaluation of REBCO superconducting joint *IEEE Trans. Appl. Supercond.* **32** 6601404
[31] McIntyre P, Wu Y, Liang G and Meitzler C R 1995 Study of Nb_3Sn superconducting joints for very high magnetic field NMR spectrometers *IEEE Trans. Appl. Supercond.* **5** 238–41
[32] Swenson C A and Markiewicz W D 1999 Persistent joint development for high field NMR *IEEE Trans. Appl. Supercond.* **9** 185–8
[33] Leupold M J and Iwasa Y 1976 Superconducting joint between multifilamentary wires 1. Joint-making and joint results *Cryogenics* **16** 215–6
[34] Iwasa Y 1976 Superconducting joint between multifilamentary wires 2. Joint evaluation techniques *Cryogenics* **16** 217–9
[35] Tominaka T, Kakugawa S, Hara N and Maki N 1991 Electrical properties of superconducting joint between composite conductors *IEEE Trans. Magn.* **27** 1846–9
[36] Wen H M, Lin L Z and Han S 1992 Joint resistance measurement using current-comparator for superconducting wires in high magnetic field *IEEE Trans. Magn.* **28** 834–6
[37] Fukuzaki T, Maeda H, Matsumoto S, Yokoyama S and Kiyoshi T 2007 Study of joint resistance in Nb_3Al-NbTi superconducting joint for high field NMR *IEEE Trans. Appl. Supercond.* **17** 1435–7
[38] Cheng J, Liu J, Ni Z, Cui C, Chen S, Song S, Li L, Dai Y and Wang Q 2012 Fabrication of NbTi superconducting joints for 400-MHz NMR application *IEEE Trans. Appl. Supercond.* **22** 4300205
[39] Liu J, Cheng J, Feng Z, Wang Q, Kun C and Xian L 2013 Electrical properties of cold-pressing welded NbTi persistent joints *Cryogenics* **58** 62–67
[40] Brittles G D, Noonan P, Keys S A, Grovenor C R M and Speller S 2014 Rapid characterisation of persistent current joints by SQUID magnetometry *Supercond. Sci. Technol.* **27** 122002
[41] Ni D, Yang W, Han S, Zhu L, Zhang X, Wu B and Ma L 2014 A test system for superconducting joints based on GM cryocooler *IEEE Trans. Appl. Supercond.* **24** 9000505
[42] Kobayashi K, Nishijima G, Uchida A, Amaya M, Banno N and Kitaguchi H 2020 Development of a superconducting joint resistance evaluation system *IEEE Trans. Appl. Supercond.* **30** 9000204
[43] Banno N, Kobayashi K, Uchida A and Kitaguchi H 2021 High-temperature-tolerable superconducting Nb-alloy and its application to Pb- and Cd-free superconducting joints between NbTi and Nb_3Sn wires *J. Mater. Sci.* **56** 20197–207
[44] Banno N, Kobayashi K, Uchida A, Kitaguchi H, Takenouchi A and Watanabe M 2022 Novel Pb-free superconducting joint between NbTi and Nb_3Sn wires using high-temperature-tolerable superconducting Nb–3Hf intermedia *IEEE Trans. Appl. Supercond.* **32** 4301205
[45] Takeda Y, Nishijima G, Kobayashi K and Kitaguchi H 2023 Fabrication of Bi-2223 superconducting joint by hot-pressing process *IEEE Trans. Appl. Supercond.* **33** 6400207
[46] Nakashima T, Yamazaki K, Kobayashi S, Kagiyama T, Kikuchi M, Takeda S, Osabe G, Fujikami J and Osamura K 2015 Drastic improvement in mechanical properties of DI-BSCCO wire with novel Lamination material *IEEE Trans. Appl. Supercond.* **25** 6400705
[47] Hayashi K 2020 *SEI Tech. Rev.* **91** 68
[48] Takeda Y, Nishijima G, Inoue K, Takano Y and Kitaguchi H 2023 The effect of intermediate layer densification on the critical current of a Bi-2223 superconducting joint *Supercond. Sci. Technol.* **36** 035004
[49] Takeda Y, Tsuchiya Y and Nishijima G 2023 Interpretation of time-dependent current and resistance of HTS closed loop with superconducting joint considering flux creep *Appl. Phys. Express* **16** 093002